JOURNAL OF GUIDANCE, CONTROL, AND DYNAMICS
Vol. 17, No. 1, January–February 1994

Optimal Control of Helicopters Following Power Failure

Yoshinori Okuno*
National Aerospace Laboratory, Mitaka, Tokyo 181, Japan
and
Keiji Kawachi†
University of Tokyo, Meguro, Tokyo 153, Japan

Helicopter control procedures following power failure were investigated theoretically by applying optimal control theory. The calculated height-velocity boundaries showed good correlation with flight test results. However, several differences were observed between the optimal solutions and pilot's control usage, especially in the timing and amplitude of the collective flare before touchdown. In addition, parameters such as pilot reaction delay, collective setting during descent, the location and available field length of the landing site, and wind speed were found to have a significant effect on the success of the emergency landing. Some of these effects are not currently taken into account during certification flight tests.

Introduction

HELICOPTERS can land safely following total power failure by using autorotation. Success of this autorotative landing depends on various factors, e.g., the pilot's control technique and operating conditions such as the gross weight, altitude, and ambient air temperature.[1] However, the most essential contributing factor is a combination of the height and velocity at the moment of power failure. Flight test verification is required for certification to establish the height-velocity (H-V) boundaries over the entire operating envelope.[2] A helicopter's takeoff path must be planned to prevent violating these boundaries while simultaneously complying with field length limitations, thereby limiting the maximum weight for takeoff from a confined area.

Accordingly, many theoretical and experimental studies have investigated methods of improving helicopter flight performance in the event of a power failure.[3] Increasing the main rotor's moment of inertia showed distinct advantages in autorotative landing capability,[4] and increasing the one-engine-inoperative (OEI) power of a multi-engine helicopter was determined to greatly benefit transport category operations.[5] In addition, many concepts have been proposed that supply augmented energy using auxiliary equipment such as a tip-jet and flywheel.[6] These techniques, however, have never been implemented successfully due to weight and cost restrictions. To best utilize available rotor rotational energy, optimal control procedures following power failure have been studied.

Komoda[7] proposed an analytical method to predict the H-V boundaries utilizing a linear optimal control theory. Lee[8] analyzed optimal autorotative landing by applying a nonlinear optimization technique to a point-mass helicopter model. The present authors[9] made several modifications to this analysis model by extending it to a longitudinal rigid-body dynamic model and adding sophisticated rotor aerodynamic model. This improved method led to the present paper, which initially discusses the optimal control procedures following power failure, with emphasis placed on their comparison with the pilot's control use recorded during flight tests. Following this, several influential parameters such as the collective control during descent, landing site restrictions, and wind speed are discussed. These parameters have a significant effect on the success of the emergency landing, although they are not taken into account during the current certification flight tests.

Received May 14, 1992; presented as Paper 92-4471 at the AIAA Guidance, Navigation, and Control Conference, Hilton Head, SC, Aug. 10–12, 1992; revision received Feb. 20, 1993; accepted for publication April 4, 1993.

*Researcher, Flight Research Division. Member AIAA.
†Professor, Research Center for Advanced Science and Technology. Member AIAA.

Formulation

Equations of Motion

The equations of motion relative to a space-fixed coordinate system were described using a rigid-body dynamic model having three longitudinal degrees of freedom. The state variables are horizontal flight distance x, height loss following power failure z, horizontal flight speed u, rate of descent w, pitch attitude Θ, pitch rate q, and rotor rotational speed Ω; whereas the control variables are the main rotor collective pitch θ_0 and longitudinal cyclic pitch θ_S. The following constraints are taken into account: collective pitch range, cyclic pitch range, pitch attitude range, maximum load factor, and maximum effective angle of attack of the blade section at 75% span. The external forces include main rotor thrust T, torque Q, H-force H, longitudinal hub moment M_R, fuselage drag D_F, horizontal stabilizer lift L_H, and weight mg (see Fig. 1). The main rotor's aerodynamic characteristics were calculated using the modified blade element theory in combination with the modified momentum theory. The former theory takes into account the blade root stall effects during descent, and the latter theory extends its applicability over all operating conditions including the vortex ring state. When considering one engine failure of a twin-engine helicopter, the remaining engine's maximum power was given as a function of the pressure altitude and air temperature. The details of these dynamic and aerodynamic helicopter models are contained in Ref. 9.

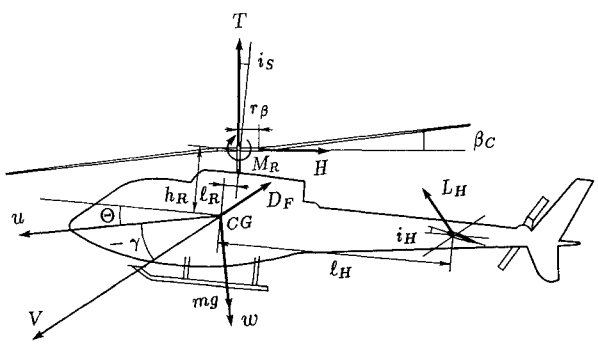

Fig. 1 Mathematical model representation.

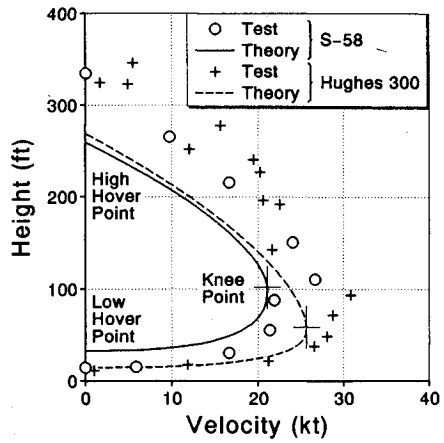

Fig. 2 Calculated H-V boundaries and flight test results.[12,13]

Optimization Problems

Four optimization problems were formulated as follows:

Problem 1) Minimizing the touchdown speed factor following power failure at a given flight condition.[9] The performance index was defined by the sum of the squares of forward speed and rate of descent at touchdown, both of which are nondimensionalized by the respective safety limits, i.e.,

$$I = \min \left\{ \left[u(t_f)/u_{\max} \right]^2 + \left[w(t_f)/w_{\max} \right]^2 \right\} \tag{1}$$

where $u_{\max} = 20$ and 30 kt for skid and wheel type helicopters, respectively, and $w_{\max} = 8$ ft/s regardless of the landing gear type.

The initial conditions were given by the state variables 0.5 ~ 1 s after power failure to simulate normal pilot reaction delay. The terminal conditions for this problem were specified to obtain level attitude at touchdown, i.e.,

$$\Theta(t_f) = 0, \qquad z(t_f) = h_0 \tag{2}$$

where h_0 is taken as the power failure height.

Problem 2) Minimizing the H-V diagram's unsafe region, which is represented by the following three points (see Fig. 2):

Problem 2a) Minimizing the high hover point height, with

$$I = \min z(t_f) \tag{3}$$

Problem 2b) Minimizing the knee point speed, with

$$I = \max_{z(t_f)} \min_{\theta_0, \theta_S} u(0) \tag{4}$$

where the knee point height $z(t_f)$ was determined so that the performance index has a stationary value.

Problem 2c) Maximizing the low hover point height, with

$$I = \max z(t_f) \tag{5}$$

The terminal conditions for problems 2a–c were specified so that the touchdown speed factor is within the safety limit, i.e.,

$$\left[u(t_f)/u_{\max} \right]^2 + \left[w(t_f)/w_{\max} \right]^2 \le 1, \qquad \Theta(t_f) = 0 \tag{6}$$

Problem 3) Minimizing the fly-away possible height in a twin-engine helicopter's H-V diagram, which is obtained by adding a 35-ft clearance above the ground to the height loss during the transition from one engine failure to level flight, i.e.,

$$I = \min z(t_f) + 35 \text{ ft} \tag{7}$$

Table 1 Helicopter specifications

Type	Max. weight, kg	Rotor radius, m	Number of engines
Sikorsky S-58	5900	8.53	1
Hughes 300	760	3.85	1
Bell 47	1290	5.66	1
Boeing Vertol YUH-61A	8500	7.47	2
MBB/Kawasaki BK117	3200	5.50	2

using the terminal conditions

$$u(t_f) \ge V_2, \qquad w(t_f) = 0 \tag{8}$$

where V_2 denotes the minimum speed to attain a 100 ft/min rate of climb.[2]

Problem 4) Maximizing the takeoff weight of a twin-engine helicopter for Category A VTOL operation,[2] which is limited to ensure the helicopter can safely return to its initial takeoff point when one engine fails during takeoff before reaching the critical decision point (CDP).[10] The performance index was given by

$$I = \min_{z(t_f)} \max_{\theta_0, \theta_S} m \tag{9}$$

where m denotes the helicopter mass. The power failure height $z(t_f)$ was determined to be the most critical height to make a safe landing, similarly as when determining the knee point height [Eq. (4)]. Since the takeoff speed in VTOL operation is negligible [$u(0) \simeq 0$], this problem is equivalent to maximizing the helicopter mass under the condition that the H-V diagram's unsafe region is eliminated.

The terminal conditions for this problem were given by Eq. (6) and, in addition, the flight distance from power failure to touchdown $x(t_f)$ was specified as a function of the power failure height $z(t_f)$ since a confined landing site is assumed in VTOL operation, i.e.,

$$x(t_f) = x_f\left[z(t_f) \right] \tag{10}$$

The maximum takeoff weight in Category A VTOL operation is consequently related to the function x_f, which in turn depends on the all engines operating (AEO) takeoff path from initial hover to the CDP (see Fig. 11).

Results and Discussion

The nonlinear optimal control problems formulated previously were solved numerically using the sequential conjugate gradient restoration algorithm.[11] The five helicopters included as examples are listed in Table 1 along with their specifications.

Single-Engine Helicopter H-V Boundary

Figure 2 shows the H-V boundaries of two single-engine helicopters, i.e., results using the presented theory (problem 2) for the Sikorsky S-58 (helicopter mass $m = 4130$ kg, density altitude $h_d = 6635$ ft) and the Hughes 300 ($m = 660$ kg, $h_d = 5000$ ft), and also their respective autorotative landing test results.[12,13] Note that under these operating conditions, the Hughes 300 has a higher knee point speed and a lower knee point height than the S-58, although their high hover point heights are almost the same. The calculated H-V boundaries are generally in good correlation with the corresponding flight test results. However, several discrepancies exist, especially in the high hover points of both the S-58 and Hughes 300 and also the low hover point of the S-58, which are primarily caused by the difference between the optimal solutions and the pilot's control use as mentioned later.

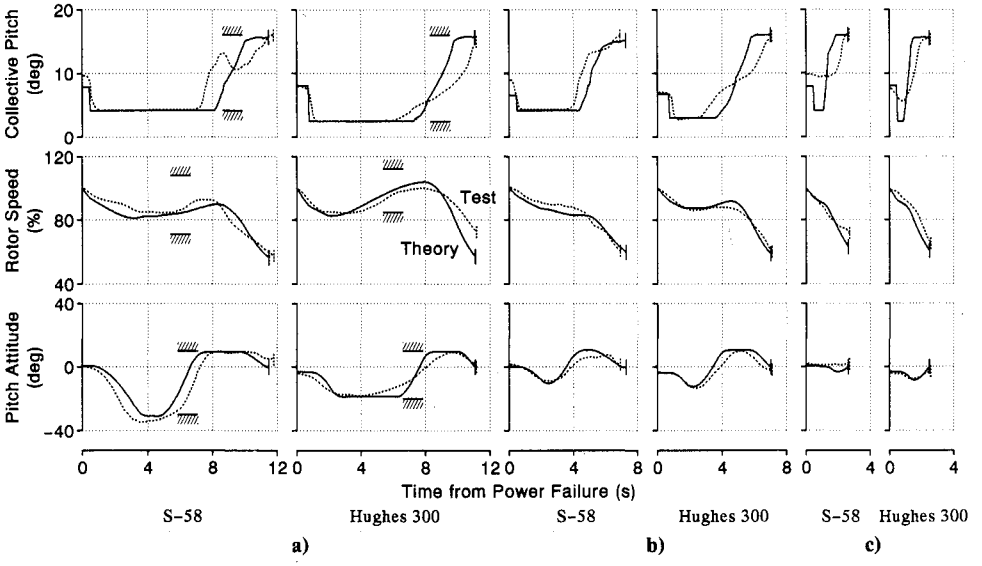

Fig. 3 Time histories of the optimal solutions and flight test results: a) high hover point, b) knee point, and c) low hover point.[12,13]

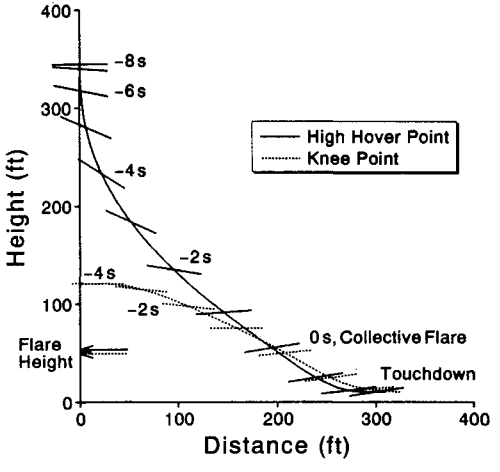

Fig. 4 Optimal landing trajectories and associated tip-path plane control histories for the S-58.

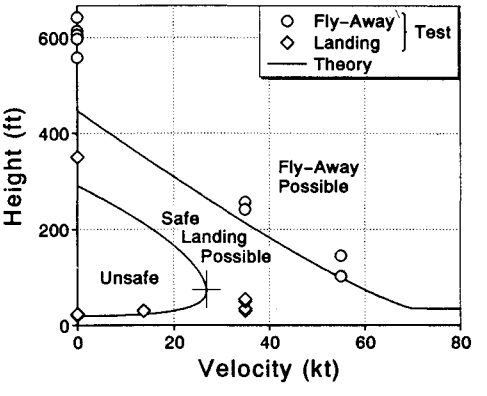

Fig. 5 Calculated H-V boundaries and flight test results for the YUH-61A.[15]

Figure 3 shows the time histories of the flight test results and optimal solutions (problem 1, the initial flight conditions were those from the flight tests) when landing from three representative points on the H-V boundary. The hatched lines indicate the allowable ranges of the collective pitch, rotor speed, and pitch attitude. Note that the rotor speed limitations (prescribed in the flight manual) are not taken into account in the optimal solutions. Since the pitch attitude limitation is a state variable constraint, it was transformed into a state and control variable constraint by introducing "slack variables."[14] The calculated optimal pitch attitude histories are generally in good agreement with the flight test results. However, some differences are observed between the calculated and measured collective pitch histories, especially when landing from the high hover point (see Fig. 3a). The S-58 pilot started the collective flare earlier than the optimal timing and then lowered the collective pitch after the initial overcontrol. On the other hand, the Hughes 300 pilot used a lower collective pitch than the optimal solution almost throughout the flare. This insufficient collective flare resulted in a higher rotor rotational energy remaining unused at the moment of touchdown. Such nonoptimal timing and amplitude of the collective flare caused the flight test high hover points to be higher than the presented theory's results (see Fig. 2).

When landing from the knee point (see Fig. 3b), both pilots performed nearly optimal collective flare, thereby obtaining good agreement with the calculated knee point heights and velocities (see Fig. 2).

When landing from the low hover point (see Fig. 3c), the S-58 pilot maintained the collective until the flare was initiated. As a result, the flight test low hover point is much lower than the calculated one (see Fig. 2). In contrast, the Hughes 300 pilot lowered the collective before raising it for the flare, showing reasonable agreement with the calculated low hover point height.

Figure 4 shows the optimal landing profiles along with the associated tip-path plane control histories when landing from the high hover and knee points of the S-58 (the numerals denote time after collective flare initiation). Note that the optimal height to start the collective flare is almost the same in both cases, but the flight-path angle and rate of descent at that moment are much different. The steep landing at a high rate of descent from the high hover point possibly prompted the pilot's collective flare.

Twin-Engine Helicopter H-V Boundary

Figure 5 shows the H-V boundaries of a twin-engine helicopter (Boeing Vertol YUH-61A, $m = 7370$ kg, $h_d = 7130$ ft),

where both the OEI fly-away and landing test results[15] are shown with the presented theory's results. It is demonstrated that this theory predicts the fly-away possible region as well as the unsafe region, although it estimates a lower minimum height for fly away following one engine failure during hover than the flight test results.

Figure 6 shows the time histories of this case, i.e., transition from one engine failure during hover to level flight (problem 3). It can be seen that the pilot performed a pitch-up maneuver earlier than the optimal timing, thus resulting in insufficient forward speed and a long duration of descending flight. The broken lines show the result of this nonoptimal control when simulated using the present helicopter math model as follows: 1) time histories of the pitch attitude and rotor rpm were prescribed so that the flight test results are simulated; 2) the collective and cyclic pitch controls were calculated to comply with these prescribed state variables; and 3) the responses of the other state variables were calculated using these control inputs. The forward speed and height loss histories obtained in this way reasonably correlate with the flight test results, hence demonstrating the fidelity of this math model.

Collective Control Effects

The standard recovery procedure in the event of a total power failure is to lower the collective immediately and maintain it at its minimum position until the flare. Therefore, the time delay before control actuation and setting of the collective pitch lower limit have significant effects on the safety and pilot workload during the autorotative landing. According to the regulations,[2] the collective pitch lower limit must be set to accommodate rotor rpm limitations in any autorotative condition without exceptional piloting skill. A sufficiently low collective pitch limit increases the autorotative landing capability by allowing more energy to be stored in the rotor system for the flare; however, it also increases the possibility of rotor overspeeding. Here these effects on the H-V boundary were investigated.

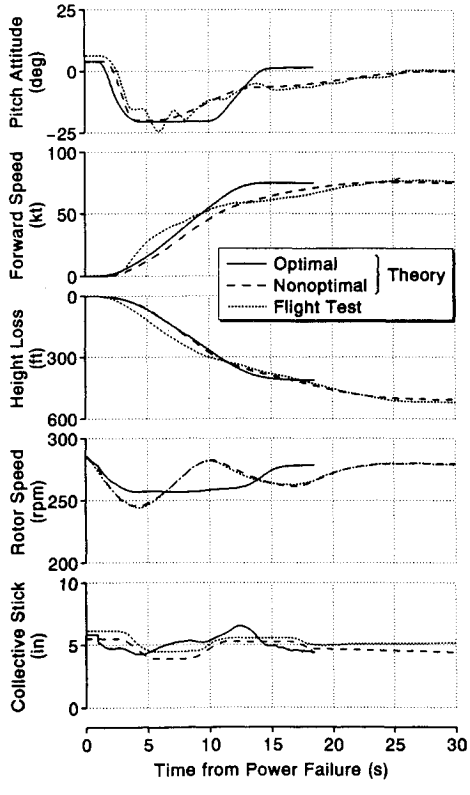

Fig. 6 Optimal and nonoptimal control histories and flight test results for the YUH-61A, fly-away from hover.[15]

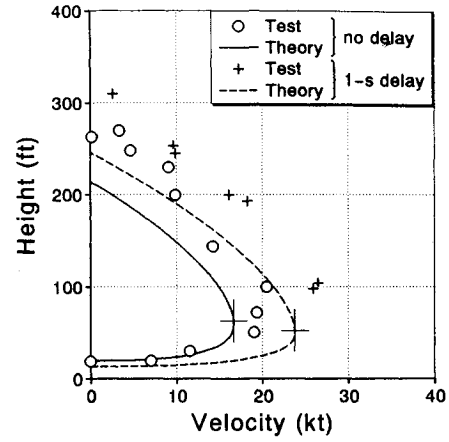

Fig. 7 Effects of pilot reaction time on the H-V boundary for the Hughes 300.

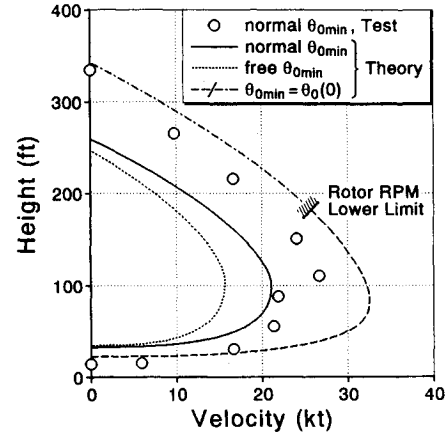

Fig. 8 Effects of collective pitch lower limit on the H-V boundary for the S-58.

Figure 7 shows the effects of the pilot reaction time on the H-V boundary (Hughes 300, $m = 670$ kg, $h_d = -200$ ft). Both the experimental and theoretical results show that a 1 s delay increases the high hover point height by 30 ft and the knee point speed by 6 kt. It is demonstrated that the presented theory can quantitatively estimate the effects of the pilot reaction delay.

Figure 8 shows the theoretical effects of the collective pitch lower limit on the H-V boundary (S-58, $m = 4130$ kg, $h_d = 6635$ ft). The dotted line shows the presented theory's results when the collective pitch lower limit was omitted. (Actually a -2 deg limit was found to be adequate since no optimal solutions violated this limitation.) A sufficiently low collective pitch limit reduces the unsafe region, especially at the knee point, because it enables rapid descent and maintains the rotor rotational energy available for the flare. When the initial height is sufficiently high (e.g., at the high hover point), the rotor rpm can be recovered during descent so that the effect of lowering the collective pitch limit is less remarkable.

The presented theory's results are additionally shown using the assumption that the initially trimmed collective pitch is maintained until the flare (broken and one dot chain lines). These results indicate the maximum effects of both the pilot reaction delay and setting of the collective pitch lower limit. Note that the flight test low hover point is reasonably estimated using this assumption since the pilot did not lower the collective following power failure as previously discussed (see Fig. 3c). However, this control technique is not generally applicable (see Ref. 16) because it significantly increases the unsafe region and also produces a region in which violating the

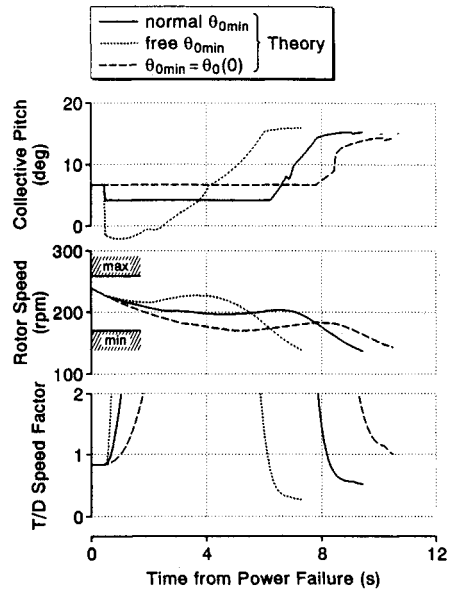

Fig. 9 Effects of collective pitch lower limit on the optimal control histories for the S-58.

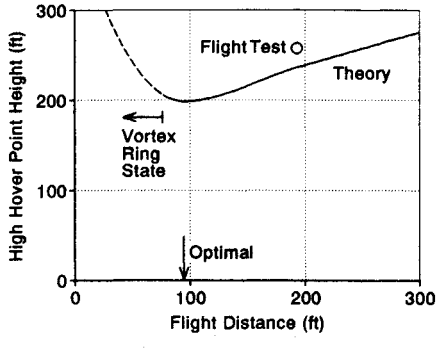

Fig. 10 Effects of flight distance on the high hover point height for the Bell 47.

rotor rpm lower limit is unavoidable as indicated by the one dot chain line.

Figure 9 shows the time histories of the optimal solutions (problem 1) using three collective pitch lower limits. The initial conditions [$h_0 = 180$ ft and $u(0) = 25$ kt, i.e., hatched area in Fig. 8] are determined so that the rotor rpm decreases to its lower limit and the touchdown speed factor is also at its limit ($= 1$) when the initial collective pitch is maintained until the flare (broken line). Note that a sufficiently low collective pitch limit (dotted line) significantly decreases the touchdown speed factor, provided proper collective pitch control is continuously performed from power failure to touchdown. The normal collective pitch lower limit (solid line) is shown to appropriately trade off between the pilot workload and the safe autorotative landing capability.

Landing Site Restriction Effects

In the current regulations,[2] it is not required to take into account the landing site restrictions, e.g., landing site location and its available field length during certification flight tests. These factors, however, have a significant effect on the success of the emergency landing in actual operation.

Figure 10 shows the theoretical effects of the flight distance from power failure to touchdown on the high hover point height of the Bell 47 helicopter ($m = 1200$ kg, $h_d = -140$ ft). The high hover point height shows a nearly linear response to the flight distance when the landing site is far enough from the power failure point. When the landing site is located close to the power failure point, a steep descent at a low forward speed is required, causing an increased high hover point height and also producing a region in which control difficulty may occur during the collective flare due to the vortex ring state[9] (broken line). Remember that this result assumes that the flight path is restricted in a vertical plane. If a spiral flight can be performed with sufficient precision, the helicopter may be safely landed even when power fails directly above the landing site. A flight test result[17] is also shown, where it can be seen that the pilot took a longer flight distance than the theoretical optimum, possibly because the steep landing of the optimal solution makes encountering the vortex ring state possible and also

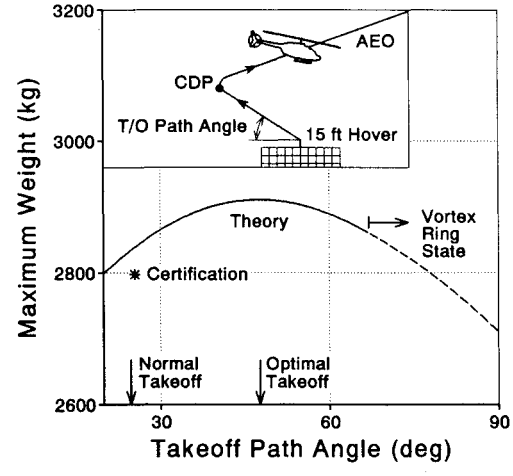

Fig. 11 Effects of the takeoff path angle on the maximum weight for the BK117 Category A VTOL operation.

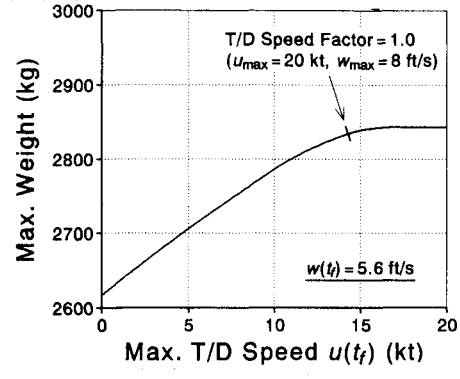

Fig. 12 Effects of the maximum touchdown speed during a rejected takeoff on the maximum weight for the BK117 Category A VTOL operation.

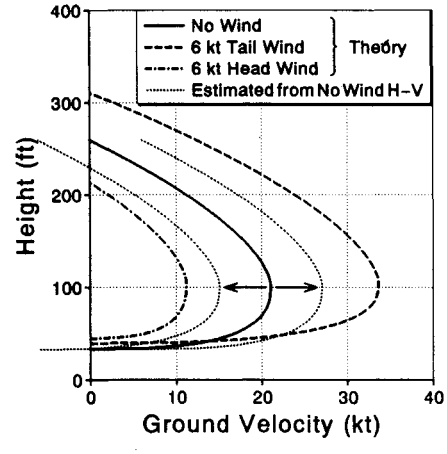

Fig. 13 Effects of wind on the H-V boundary for the S-58.

makes keeping the landing site in view difficult for the pilot. The measured and calculated high hover point heights show good agreement at the flight test flight distance.

The flight distance from power failure to touchdown is most severely limited during a rejected takeoff in Category A VTOL operation at a confined heliport. The VTOL takeoff is usually performed using a linear rearward path from initial hover to the CDP so that the pilot can keep the heliport in view (see Fig. 11). Hence, the angle of this takeoff path determines the relationship between the power failure height and the distance to be flown to the landing site [i.e., function x_f in Eq. (10)], which consequently influences the maximum takeoff weight (problem 4). The solid and broken lines in Fig. 11 show the theoretical effect of this takeoff path angle on the maximum weight for Category A VTOL operation (BK117, $h_d = 2000$ ft). The normal takeoff path angle prescribed in this helicopter's flight manual is also indicated, at which the calculated maximum weight shows reasonable agreement with the certified weight. The optimal takeoff path angle increases the theoretical maximum weight by nearly 80 kg, although such a steep takeoff reduces the pilot's visibility of the heliport.

Not only the flight distance but also the touchdown speed would be severely limited during a rejected takeoff in a confined area, e.g., a pinnacle helipad. Figure 12 shows the theoretical effects of the maximum horizontal touchdown speed $u(t_f)$ on the maximum weight when assuming the normal takeoff path angle. Here the vertical touchdown speed $w(t_f)$ is fixed at 5.6 ft/s, which is the calculated result when using the normal touchdown speed limitations of $u_{\max} = 20$ kt and $w_{\max} = 8$ ft/s in Eq. (6). Results indicate the landing site should be long enough to accommodate a 15 kt horizontal touchdown speed so that the weight limitation is maximized. Alternatively, more than 200 kg must be off-loaded if the heliport is so small as to require a zero horizontal touchdown speed.

Wind Effects

Clearly defining wind effects on helicopter power failure safety by means of flight tests is difficult. Accordingly, these effects were investigated theoretically here assuming steady and uniform wind conditions.

Figure 13 shows the wind effects on the H-V boundary of the S-58 helicopter. Note that these results are given as a function of ground speed. Because the state variable u is defined as airspeed, the wind effects can be estimated by shifting the no-wind H-V boundary to correspond with the wind speed as shown by the dotted lines, provided that the touchdown speed limitation in Eq. (6) is also defined by airspeed. In actual operations, however, the touchdown speed limitation must be determined relative to the ground, hence Eq. (6) was rewritten as follows:

$$\left\{\left[u(t_f) + u_w\right]/u_{\max}\right\}^2 + \left[w(t_f)/w_{\max}\right]^2 \le 1 \qquad (11)$$

where u_w denotes the wind speed (positive tail wind). The broken and one dot chain lines show the presented theory's results using this assumption for 6 kt tail and head winds, respectively. Note that the 6 kt tail wind increases the high hover point height by 50 ft and the knee point speed by 12 kt.

Conclusions

A theoretical method based on optimal control theory was successfully applied to investigate helicopter safety following power failure. It was demonstrated that the presented theory predicts the single- and twin-engine helicopters' H-V boundaries with reasonable correlation to flight test results. However, several differences were observed between the optimal solutions and pilot's control usage, especially in the timing and amplitude of the collective flare before touchdown. It was also pointed out that success of the emergency landing significantly depends on parameters such as the collective control delay, collective setting during descent, location and available field length of the landing site, and wind speed.

References

[1]Pegg, R. J., "An Investigation of the Helicopter Height-Velocity Diagram Showing Effects of Density Altitude and Gross Weight," NASA TN D-4536, 1968.

[2]"Airworthiness Standards: Transport Category Rotorcraft," Federal Aviation Regulations Part 29, Federal Aviation Administration, U.S. Dept. of Transportation, 1985.

[3]Studwell, R. E., "Helicopter Dynamic Performance Program. Volume 1: Engineer's Manual," USARTL-TR-79-27A, U.S. Army Research and Technology Laboratories, Fort Eustis, VA, 1980.

[4]Dooley, L. W., and Yeary, R. D., "Flight Test Evaluation of the High Inertia Rotor System," USARTL-TR-79-9, U.S. Army Research and Technology Laboratories, Fort Eustis, VA, 1979.

[5]Semple, R. D., Yost, J. H., King, E. W., Gonsalves, J. E., and Thompson, W., "Emergency Power Benefits to Multi-Engine Helicopters," *Journal of the American Helicopter Society,* Vol. 22, No. 3, 1977, pp. 27–33.

[6]White, G. T., Logan, A. H., and Graves, J. D., "An Evaluation of Helicopter Autorotation Assist Concepts," *Proceedings of the 38th Annual Forum of the American Helicopter Society,* American Helicopter Society, Washington, DC, May 1982, pp. 194–216.

[7]Komoda, M., "Prediction of Height-Velocity Boundaries for Rotorcraft by Application of Optimizing Techniques," *Transactions of the Japan Society for Aeronautical and Space Sciences,* Vol. 15, No. 30, 1973, pp. 208–228.

[8]Lee, A. Y., "Optimal Autorotational Descent of a Helicopter with Control and State Inequality Constraints," *Journal of Guidance, Control, and Dynamics,* Vol. 13, No. 5, 1990, pp. 922–924.

[9]Okuno, Y., Kawachi, K., Azuma, A., and Saito, S., "Analytical Prediction of Height-Velocity Diagram of a Helicopter Using Optimal Control Theory," *Journal of Guidance, Control, and Dynamics,* Vol. 14, No. 2, 1991, pp. 453–459.

[10]Okuno, Y., and Kawachi, K., "Optimal Takeoff of a Helicopter for Category A V/STOL Operations," *Journal of Aircraft,* Vol. 30, No. 2, 1993, pp. 235–240.

[11]Wu, A. K., and Miele, A., "Sequential Conjugate Gradient Restoration Algorithm for Optimal Control Problems with Non-Differential Constraints and General Boundary Conditions, Part 1," *Optimal Control Applications and Methods,* Vol. 1, 1980, pp. 69–88.

[12]Hanley, W. J., DeVore, G., and Martin, S., "An Evaluation of the Height Velocity Diagram of a Heavy Weight, High Rotor Inertia, Single Engine Helicopter," FAA-ADS-84, Federal Aviation Administration, Washington, DC, 1966.

[13]Hanley, W. J., and DeVore, G., "An Evaluation of the Height Velocity Diagram of a Light Weight, Low Rotor Inertia, Single Engine Helicopter," FAA-ADS-46, Federal Aviation Administration, Washington, DC, 1965.

[14]Jacobson, D. H., and Lele, M. M., "A Transformation Technique for Optimal Control Problems with a State Variable Inequality Constraint," *IEEE Transactions on Automatic Control,* Vol. AC-14, No. 5, 1969, pp. 457–464.

[15]Benson, G., Bumstead, R., and Hutto, A. J., "Use of Helicopter Flight Simulation for Height-Velocity Test Predictions and Flight Test Risk Reduction," *Proceedings of the 34th Annual Forum of the American Helicopter Society,* American Helicopter Society, Washington, DC, Paper 41, May 1978.

[16]Pegg, R. J., "A Flight Investigation of a Lightweight Helicopter to Study the Feasibility of Fixed-Collective-Pitch Autorotations," NASA TN D-5270, 1969.

[17]Hanley, W. J., and DeVore, G., "An Evaluation of the Effects of Altitude on the Height Velocity Diagram of a Single Engine Helicopter," FAA-ADS-1, Federal Aviation Administration, Washington, DC, 1964.